



**HAL**  
open science

## Enhancing aqueous dispersibility of uncharged cellulose through biosurfactant adsorption

Thuy-Linh Phi, Wenyang Xu, Petra Pernot, Niki Baccile, Eero Kontturi

► **To cite this version:**

Thuy-Linh Phi, Wenyang Xu, Petra Pernot, Niki Baccile, Eero Kontturi. Enhancing aqueous dispersibility of uncharged cellulose through biosurfactant adsorption. 2024. hal-04764723

**HAL Id: hal-04764723**

**<https://hal.science/hal-04764723v1>**

Preprint submitted on 4 Nov 2024

**HAL** is a multi-disciplinary open access archive for the deposit and dissemination of scientific research documents, whether they are published or not. The documents may come from teaching and research institutions in France or abroad, or from public or private research centers.

L'archive ouverte pluridisciplinaire **HAL**, est destinée au dépôt et à la diffusion de documents scientifiques de niveau recherche, publiés ou non, émanant des établissements d'enseignement et de recherche français ou étrangers, des laboratoires publics ou privés.

# Enhancing aqueous dispersibility of uncharged cellulose through biosurfactant adsorption

*Thuy-Linh Phi,<sup>a,b</sup> Wenyang Xu,<sup>a</sup> Petra Pernot,<sup>c</sup> Niki Baccile,<sup>b,\*</sup> Eero Kontturi<sup>a,\*</sup>*

<sup>a</sup> Department of Bioproducts and Biosystems, School of Chemical Engineering, Aalto University, P.O. Box 16300, 00076 Aalto, Finland

<sup>b</sup> Sorbonne Université, Centre National de la Recherche Scientifique, Laboratoire de Chimie de la Matière Condensée de Paris, LCMCP, F-75005 Paris, France

<sup>c</sup> ESRF – The European Synchrotron, 38043 Grenoble, France

## **Keywords**

cellulose nanocrystal, biosurfactant, colloidal stability, microcrystalline cellulose

## **Abstract**

Cellulose, the principal structural ingredient in plant cell wall, holds promise for a range of bio-based high-tech applications. Acid (e.g., HCl) hydrolysis of cellulose microfibrils leads to cellulose nanocrystals (CNCs), which are commonly suspended in water by repulsive interactions introduced with negative charges after a sulfuric acid treatment or TEMPO oxidation. Lack of surface charges prompts CNCs sedimentation. This work addresses the dispersibility of uncharged cellulose nano- and micro- particles (CNCs and microcrystalline cellulose, MCCs) in water through the physical adsorption of a glycolipid biosurfactant, composing of a single-glucose moiety and a fatty acid tail. The methodology involves the sonication-assisted incorporation of the biosurfactant directly within HCl hydrolyzed cellulose, without any surface modification (TEMPO oxidation or sulfation). Characterization of biosurfactant-stabilized cellulose reveals an enhancement in water stability of MCCs and CNCs in time at room temperature up to at least one day. These results show that adsorption of glycolipid biosurfactants are an interesting approach to disperse uncharged cellulose, potentially expanding its use in various technological domains.

## 1. Introduction

Cellulose nanocrystals (CNCs) are rigid, nanosized rods that can be isolated from plant-based fibers by acid hydrolysis. They are a premium example of modern-day nanoparticles, whose assets include renewability, biodegradability, and bio-based origin.<sup>1-3</sup> Although originally introduced 75 years ago,<sup>4</sup> particularly the past two decades have seen CNCs explored in a wealth of materials applications in the fields of composites,<sup>5</sup> structural color,<sup>6</sup> biomedical, or catalysis.<sup>7,8</sup> Industrial production of CNCs has also gathered momentum with several pilot plants and commercial sites introduced around the globe in the past 15 years.

As with any nanoparticle, if CNCs are to be used efficiently, they need to be well-dispersed in water for most applications. The usual route to dispersion is to introduce charge on the CNCs surface. An overwhelming majority of studies as well as the industrial processes utilize sulfuric acid hydrolysis for CNCs isolation, which simultaneously introduces charged sulfate half-esters on the surface of the crystal.<sup>9,10</sup> While the method works well, it is based on a study published in 1953<sup>11</sup> and suffers from drawbacks, such as low yield, high water consumption, and poor recyclability of the acid.<sup>12-14</sup> Furthermore, the sulfate groups can act as autocatalyst, decreasing the thermal stability of CNCs.<sup>15,16</sup> Uncharged CNCs, by contrast, can be produced in principle just by HCl hydrolysis but their isolation is insufficient: instead of CNCs, the incomplete dispersion after HCl hydrolysis leads to microcrystalline cellulose (MCCs) that consists predominantly of micron-sized particles. The MCC particles can potentially be dispersed into CNCs but this often results in low yields and polydisperse particle size (Figure 1a).<sup>17-19</sup> The purpose of this study is to explore an uncharted route, that is, the use of a biosurfactant, to facilitate the dispersion of a hydrolyzed cellulose substrate into CNCs.

To turn uncharged, hydrolyzed cellulose to a colloiddally stable dispersion, the most commonly used method is introducing surface charge by chemical reactions, such as esterification<sup>20-22</sup> or oxidation.<sup>23-25</sup> Non-covalent methods generally minimize the need for chemical reagents, solvents, and laborious purification steps. It takes a simple mixing step of the hydrolyzed cellulose with various water-soluble polysaccharides and oligomers.<sup>26,27</sup> Surfactants – the most common dispersing agents in colloid science – have received less attention as CNCs dispersants, mainly because they do not work as expected, largely due to their poor affinity to cellulose. The early accounts utilized specific surfactants to alleviate CNCs dispersion in hydrophobic solvents.<sup>28,29</sup> More recently, Shang et al. observed that CTAB, at the concentration over its critical micellar

concentration ( $>0.5$  mM), promotes the aggregation of CNCs, due to the self-assembly properties of the surfactant. Their team also found out that a lower concentration of CTAB (0.13–0.47 mM) was able to stabilize uncharged CNCs for up to 7 days. Separate investigations used sorbitan monostearate for adsorption on uncharged CNCs surfaces, noting a brief improvement in dispersion (for a few minutes) that diminished with increased surfactant, likely due to micelle formation.<sup>30</sup> In a 2017 review, Tardy et al. pointed out that, despite the extensive potential of surfactants in modifying nanocellulose surfaces, progress has been limited and mostly concentrated on practical applications in the last 20 years.<sup>31</sup>

In another parallel field of research, surfactants of biological origin have recently gained significant attention. The rising demand for environmentally friendly and effective surfactants in sectors such as agriculture, cosmetics, food, pharmaceuticals, and environmental protection has steered the focus towards the use of microbial sources to produce surfactants.<sup>32,33</sup> Due to their intriguing structure, microbial biosurfactants are increasingly recognized for versatile applications.<sup>34,35</sup> Inspired by the natural affinity towards cellulose surfaces of diverse saccharides like glucose, cellobiose,<sup>36</sup> oligosaccharides, and cello-oligosaccharides,<sup>37,38</sup> as well as dendrons with sugar units,<sup>39</sup> we have adopted a strategy of using glucose-based biological amphiphiles. The selected amphiphile is a single-glucose lipid named G-C18:1 (Figure 1b) which belongs to the family of microbial biosurfactants, produced by fermentation and has two major advantages concerning synthetic surfactants, including alkylpolyglycosides. First, microbial fermentation guarantees monodispersity of the hydrophilic headgroup, in this case, a single sugar, known to have a good affinity towards cellulose.<sup>36</sup> Second, most biosurfactants, including G-C18:1, have a double amphiphilic, bolaform, molecular structure, of which one end is composed of a free-standing carboxylic acid unit. The hypothesis is then that the double functionality enhances adsorption onto cellulose surface (glucose binding) and improved colloidal stability (charge introduction). With unique chemical properties, biosurfactants promise a new level of control over CNCs dispersion. Biosurfactants – with their tunable structures – could then provide a key to unlock the full potential of CNCs in water while keeping their sustainability high, presenting a green approach for dispersing uncharged hydrolyzed cellulose in both scientific research and industrial applications.

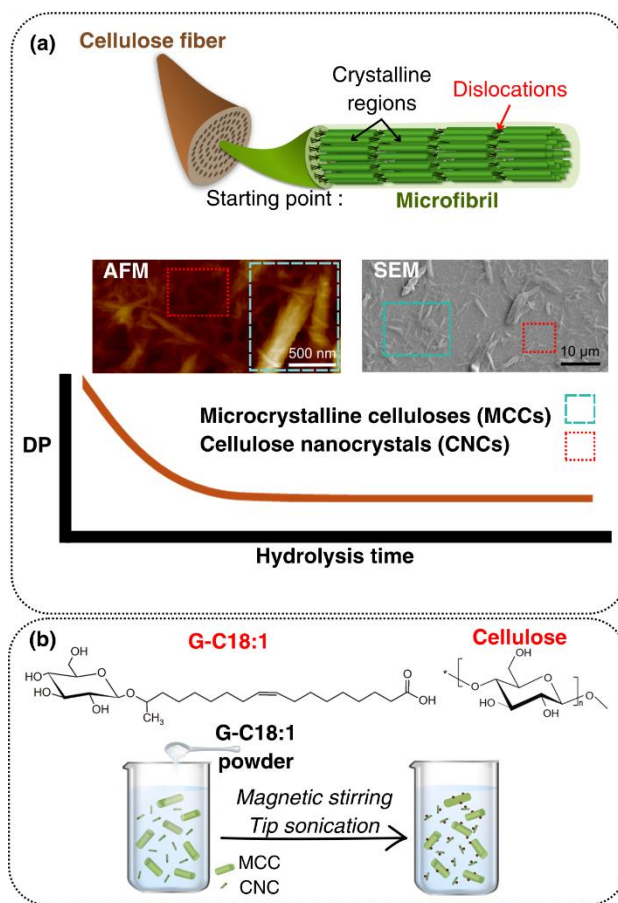


**Figure 1. (a)** Cellulose fibers, which comprise both crystalline areas and non-crystalline segments, are subjected to acid hydrolysis to eliminate the dislocations. The size of the resulting cellulose crystalline particles can range from microns (MCCs) to nanometers (CNCs). **(b)** Simplified illustration of the sample preparation involving the combination of cellulose and the glucolipid biosurfactant and their chemical structures.

## 2. Results

Aqueous HCl hydrolysis of cotton linters (Whatman 1), reaching the leveling-off degree of polymerization (LODP),<sup>40</sup> produced both micron-sized MCCs and nanosized CNCs (Figure 1a). Therefore, from now on, the cellulose in our sample will be referred to as hydrolyzed cellulose (HC), as it is a mixture of both MCCs and CNCs. The biosurfactant G-C18:1 (Figure 1b), consisting of a glycosyl headgroup linked to a monounsaturated C18 fatty acid, was used to disperse the uncharged, crystalline cellulose. G-C18:1 with its unique double amphiphile (glucose headgroup and carboxylic end-group) character, differentiates itself from conventional surfactants both in structure and self-assembly properties.<sup>41</sup> At concentrations below about 10 wt%, G-C18:1 assembles into micelles above pH 7, vesicles below pH 6.2, wormlike micelles in the transition

pH range and lamellar precipitate below pH 4,<sup>42,43</sup> whereas its critical micelle concentration (CMC) was reported to be between 0.07 mg/mL and 0.12 mg/mL (0.16-0.26 mM) at physiological pH and 0.035 mg/mL (0.08 mM) at pH 3.<sup>44-46</sup> In the present study, the critical aggregation concentration (CAC) is preferred to the more standard CMC, due to broader morphological variety of the G-C18:1 aggregates.<sup>41</sup> According to dynamic light scattering (DLS) performed over a broader range of concentrations in the pH domain of vesicles stabilization (between pH 4.5 and 5) (Figure S1), we found a more complex behavior than expected, when compared to the literature.<sup>44-46</sup> At first, an increase in scattering occurs between 0.02 mg/mL (0.04 mM) and 0.03 mg/mL (0.06 mM), a range that is in very good agreement with the values reported at pH 3, and most likely corresponding to a monomer-to-micelle, or monomer-to-cluster transition. Nevertheless, we also observe a second event at higher concentrations,  $0.47 \pm 0.01$  mg/mL (1 mM), probably corresponding to an increase in size, as commonly reported for second CMCs,<sup>47</sup> or to a change in morphology (micelle-to-vesicles), as expected for this compound at pH between 4 and 6.2.<sup>42,43</sup> Both hypotheses are most likely true, because elongated micelles are a well-known intermediate shape between spherical micelles and vesicles, as reported for lecitin-bile salts as a function of concentration<sup>48</sup> and for G-C18:1 itself as a function of pH.<sup>42</sup>

The range of G-C18:1 concentrations used for the stabilization of HC was eventually chosen on the basis of the amount theoretically required to coat a single CNC crystal. The theoretical surface area of CNCs was evaluated to be between 400 m<sup>2</sup>/g and 500 m<sup>2</sup>/g, that is, between 4 and 5·10<sup>22</sup> Å<sup>2</sup>/g.<sup>49,50</sup> Considering that the area per molecule for G-C18:1 was reported to be 35 Å<sup>2</sup> and 47 Å<sup>2</sup>,<sup>51</sup> and more globally between 40 Å<sup>2</sup> and 50 Å<sup>2</sup> for single glucose lipids,<sup>52,53</sup> one estimates a mass range between 0.6 g and 0.8 g of G-C18:1 to equalize the specific surface area of CNCs. This range is actually in agreement with the experimental value of 0.7 g reported for the commercial Beycostat NA surfactant.<sup>54</sup> Given the above, to set ourselves in the full coverage domain of the HC (1 mg/mL), we have chosen to study the stabilization effect of G-C18:1 both above and below its second CAC (Figure S1), that is, at concentrations between 0.2 and 1.0 mg/mL (corresponding sample names are Sample 0.2 to Sample 1, Table S1).

## 2.1. Colloidal stability

Two methods were tested to mix G-C18:1 and hydrolyzed cellulose (HC): combining their aqueous solutions or adding G-C18:1 powder directly to the HC solution (Figure S2) (pH ~ 4.5). The latter

method (Figure 1b) proved to be more effective for colloidal stability and preventing sedimentation. Turbidity was used to monitor the sedimentation kinetics of all samples (Figure 2a). Over time, it showed that while cellulose alone (referred to as Sample 0) completely sedimented within two hours, G-C18:1-infused samples (Sample 0.2 to Sample 1) remained stable over days (Figure 2b and Figure S3), underscoring the stabilizing role of the biosurfactant. This is notable as HCl-hydrolyzed cellulose typically aggregates heavily due to a lack of surface stabilization.<sup>55</sup> Sedimentation process of these samples was monitored for three weeks until stability was achieved (Figure 2c). By fitting the decay with a simple exponential, one can quantify the time constants shown in Figure 2d. The presence of biosurfactant increases the stability in time of HC up to a factor of 30, as in Sample 0.4. Interestingly, the concentration of G-C18:1 around its CAC provided the best colloidal stability to the system. That piece of information is confirmed by the time-lapse images of the cellulose and biosurfactant mixture in Figure 2e. Starting at 0.2 mg/mL of G-C18:1 (Sample 0.2), a dense, opaque phase emerges and settles more slowly than the cellulose alone, suggesting that the biosurfactant helps in maintaining the cellulose in a swollen state within the solution. For samples where the G-C18:1 concentration is below the CAC, the supernatant appears to be clear. Above the CAC (from Sample 0.4 onward), the supernatant appeared turbid, a phenomenon rather attributed to the well-known vesiculation properties of G-C18:1 itself at pH below neutrality<sup>42,43</sup> than to the dispersion of cellulose itself (Figure S4). To better understand the origin of the enhanced stability, we performed zeta potential measurements (Figure 2f). Indeed, stabilization by electrostatic repulsion forces is the classical mechanism reported for TEMPO or sulfuric acid treated CNCs. In the present system, G-C18:1 contains a free-standing carboxylic acid group, partially ionized at pH ~ 5, considering a pKa= 5.7 for G-C18:1.<sup>46</sup> Zeta potential measurements revealed that adding G-C18:1 reduced the zeta potential from  $-10.7 \pm 5.15$  mV to  $-17.7 \pm 3.77$  mV. The initial negative charge, a result to be taken with care considering the large relative error (50 %) from 6 measurements (Figure S5), correlates with previous accounts.<sup>31,56</sup> The decreased zeta potential with smaller relative error (21%),  $-17.7 \pm 3.77$  mV, indicates that the increased stability could be related to the presence of the deprotonated form of G-C18:1 on the HC surface (Figure 2f). While the zeta potential values of -10 mV and -17 mV both fall within the range typically associated with incipient instability,<sup>57</sup> the observed decrease in the magnitude of the zeta potential after the addition of glucolipid is still indicative of improved stability. This is supported by the longer-term stability observed in the samples

containing glucolipid. It suggests that the glucolipid has a surface stabilizing effect on HC particles through electrostatic repulsive forces. The zeta potential values, yet negative, are still lower in absolute value than those measured for CNCs modified with TEMPO (approximately  $-60\text{ mV}$ )<sup>58</sup> or sulfuric acid (ranging from  $-30$  to  $-40\text{ mV}$ )<sup>59</sup>.

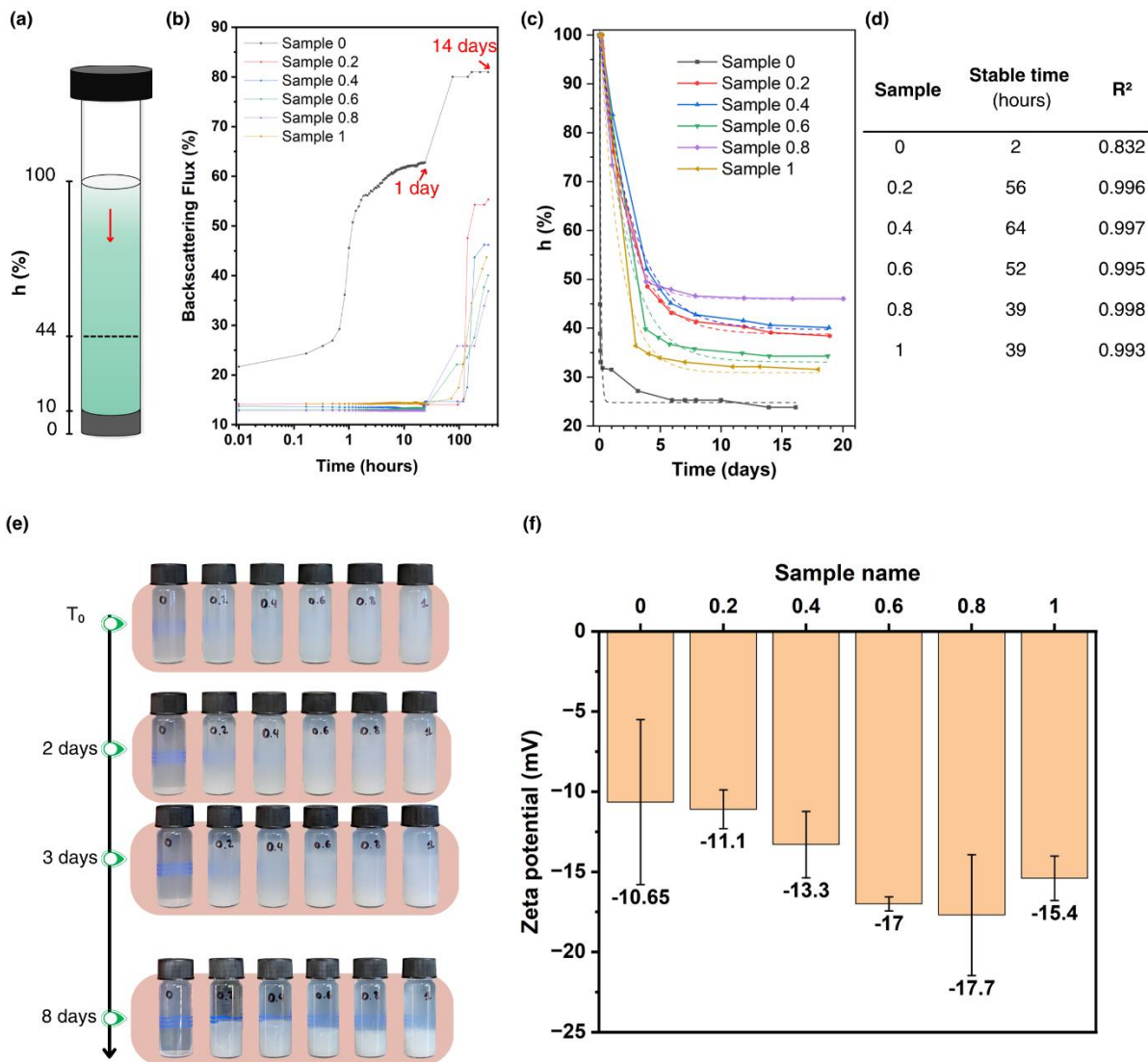


Figure 2. (a) Illustration of the typical Turbiscan vial. The height ( $h$ ), which changes in time, corresponds to the distance comprised between the bottom of the vial and the meniscus; (b) backscattering profile recorded at  $h = 44\%$  of the samples during 2 weeks; (c) the sedimentation height tracked up to 20 days and fitted using a single exponential decay to determine sedimentation time constant, reported in in (d); (e) time-lapse images of the cellulose and biosurfactant mixture and (f) zeta potential measurements of the samples (error is calculated over 3 samples).

## 2.2. Structural characterization

Small-angle X-ray scattering (SAXS) measured within the  $q$  range between  $0.07$  and  $5 \text{ nm}^{-1}$  ( $90 \text{ nm}$  and  $1.3 \text{ nm}$ ) was used as a preferential technique to probe the aggregation and morphology of both cellulose<sup>60,61</sup> and G-C18:1.<sup>41,42</sup> G-C18:1 was measured below and above its CAC2, although the concentration range of G-C18:1 used in this work was at the limit of detection of the instrument, despite the use of synchrotron radiation. As a control, the SAXS profiles of pure G-C18:1 at pH about 4.4 and between  $0.02 \text{ mg/mL}$  and  $1.0 \text{ mg/mL}$  only displayed a signal above the CAC2 ( $0.4 \text{ mg/mL}$ ) (Figure S6c). For comparison, the concentration of  $1 \text{ mg/mL}$  was also found to be at the detection limit of SAXS for aqueous solutions of other microbial glycolipids.<sup>62</sup> Despite the lack of thorough characterization of the self-assembly of G-C18:1 below  $5 \text{ mg/mL}$ , it is known that, at pH below 6.2 this compound assembles into single-membrane vesicles,<sup>42,43</sup> of which the typical scattering profile is given at  $20 \text{ mg/mL}$  in Figure S6c. The scattering profiles of G-C18:1 at  $0.4$  and  $1 \text{ mg/mL}$  at pH 4.5, also shown in Figure S6c, do confirm that G-C18:1 self-assembles at CAC2. Even if the poor signal-to-noise ratio of the signal around CAC2 does not allow a precise morphological attribution of the scattering objects, one can reasonably expect the coexistence of elongated micelles (around CAC2) and vesicles (above CAC2). Wormlike micelles are not an uncommon intermediate and they were already reported for G-C18:1 itself above CAC2, as a function of pH,<sup>42</sup> as well as for other amphiphilic systems, like lecitin-bile salts, as a function of concentration.<sup>48</sup>

After mixing HC and G-C18:1, samples were separated into two layers: referred to as supernatant (top) and sedimented (bottom) phases. The signal of the supernatant phase (Figure 3a and Figure S6a) is low and noisy, with a scattering profile being different than what should be expected for the G-C18:1 controls at pH below 6.2 and for concentrations above the CAC2 (Figure S6c). This finding shows that the supernatant phase neither contains vesicles nor micelles (spherical or wormlike). A closer look at the SAXS data of Samples 0.2 to 1 shows that for the less noisy of them (e.g., Sample 0.2, Figure 3a), a model-independent Guinier function<sup>63</sup> with a radius of gyration,  $R_g$ , of approximately  $0.6 \text{ nm}$  (sphere radius of  $0.9 \text{ nm}$ ) could fit the data. Comparison of this value to the expected radius of G-C18:1 micelles (measured at basic pH only) of  $1.4 \text{ nm}$ <sup>42,43</sup> suggests the presence of small glucolipid clusters rather than actual micelles. The SAXS profiles of the supernatant also exclude the presence of statistically-relevant amounts of crystalline cellulose, of which the presence can probably not be totally excluded on the basis of optical and

atomic force microscopy (AFM) arguments (Figure 3b) for Sample 1. Optical microscopy shows the spurious presence of large particles of about 50  $\mu\text{m}$  in size, while AFM reveals the presence of anisotropic needles of about 200 nm in length (arrows in AFM image in Figure 3b), reasonably attributed to MCCs and CNCs respectively.<sup>64</sup> The latter seems to be embedded in a continuum-dense, featureless matrix deposited on the AFM substrate, of which the nature could well be attributed to G-C18:1. Eventually, if one cannot exclude, according to AFM, that cellulose and glucolipids are in the supernatant, the SAXS data demonstrate that their content is negligible, hence suggesting their strong interaction with HC in the bottom phase.

For the sedimented phase, SAXS, optical microscopy, and AFM investigations are shown in Figure 3a and Figure 3b. The SAXS profile of the commercial sulfate-stabilized CNC control sample (Figure 3a) can be fitted with a classical parallelepiped form factor model.<sup>60</sup> The values of the parallelepiped height,  $h= 5.0$ , and width,  $w= 21.3$ , obtained from the fitting process (refer to the SAXS section in the Supporting Information for more details) match well with the data reported by Grachev et al. for a series of CNC sample dispersions.<sup>60</sup> The typical SAXS curve of the G-C18:1/cellulose sub-phase is shown in Figure 3a for Sample 0.2 only, as all other samples (Figure S6b) have the same profile. All samples display a scattering profile that is comparable with the control CNCs only and different from the signals of G-C18:1 alone or HC. If G-C18:1 self-assembled structures were in suspension, one would indeed observe an oscillation of the form factor above  $1 \text{ nm}^{-1}$  both for vesicles (refer to control at 20 mg/mL in Figure S6b) or micelles.<sup>42,43</sup> On the other hand, the HC material (Sample 0) is characterized by a monotonous scattering with an approximate -3 slope (log-log scale, Figure 3a), typical of large fractal interfaces.<sup>65</sup> Interestingly, the SAXS profile of the G-C18:1/cellulose sample (Sample 0.2 in Figure 3a) can actually be fitted with the same parallelepiped form factor model used for the CNCs control using comparable structural parameters,  $h= 3.5 \text{ nm}$  and  $w= 19.0 \text{ nm}$  (all others fitting parameters being unchanged, see supporting information). The fit is, however, poor below  $0.1 \text{ nm}^{-1}$ , as G-C18:1/cellulose sub-phase samples exhibit a slope of about -2.5, a notable deviation from the CNC control (-1.5). At a minor extent, the fit is also poor between  $0.8 \text{ nm}^{-1}$  and  $2 \text{ nm}^{-1}$ . These features are discussed below.

Alteration in the slope at low low- $q$  could be explained by the presence of MCCs or by aggregation of CNCs. The  $I(q)$  power law dependence is generally associated to the interface scattering. When the interface is flat, the expected power law is -4, but in the case of surface or volume fractals, the

expected power law dependency varies between -4 and -3 or between -2 and -3, respectively.<sup>65</sup> A recent work by Leppänen et al. summarizes the most common power laws and fractal dimensions observed for MCCs and nanofibrillated cellulose (NFC) as well as their corresponding q-range.<sup>61</sup> As one would expect, the most common set of values is contained between -3 and -4, depending on the treatment. This is easily explained by the fact that the size of MCCs and NFC particles (microns in length) is orders of magnitude larger than the length scale probed by SAXS under standard conditions of use (0.1 to 10 nm<sup>-1</sup>, that is 63 to 0.6 nm). Deviations from -4 are generally explained by surface fractals. In this field, only few values between -1.2 and -1.9, or slightly higher than -3 (e.g., -2.7 or -2.9), were also reported and explained by the presence of mass fractals, probably induced by the alteration of the cellulose crystallites core structure by water adsorption.<sup>61</sup> Differently than MCCs and NFCs, colloidal CNCs show the typical low-q slope in the order of -1.5/-1.6, associated to the scattering signal of a parallelepiped (Figure 3a).<sup>60</sup> However, attractive interactions driving the aggregation of CNCs lead to fractal structures, which commonly explain deviation in the low-q portion of the spectra compared to the parallelepiped model (PM). Slopes of -2.3 were actually reported in a recent study,<sup>66</sup> in which authors nicely correlate the reduction in the CNCs charge density with the deviation in the SAXS profile below about 0.3 nm<sup>-1</sup>. Interestingly, the same work also shows that deviation between experimental data and PM also occur between 0.7 nm<sup>-1</sup> and 2 nm<sup>-1</sup> (note: values are given in Å<sup>-1</sup> in their work), that is the same range in which a similar deviation exists between the data and PM for the G-C18:1/cellulose sample (Sample 0.2 in Figure 3a). Considering the stronger similarity between the fitting results performed in this work and the data reported by Cherhal et al.,<sup>66</sup> one can reasonably state that the SAXS profiles of the sub-phase show that G-C18:1 interacts with hydrolyzed cellulose so as to contribute to stabilizing CNCs, which undergo partial interaction associating into CNCs mass fractals. In light of the above, when considering the SAXS and zeta potential (Figure 2f) data together, one can argue that G-C18:1 is able to stabilize individual CNCs but that the low charge density drives their aggregation at longer time scales (> 24 h).

The SAXS profiles of the G-C18:1/cellulose samples, both in the supernatant and the sub-phase, lack the signal of G-C18:1 (micellar or vesicular form), demonstrating that the glucolipid, even above the CAC2, preferentially adsorbs at the water/CNC interface. The stabilization works well when G-C18:1 is added in the powdery state to the HC suspension, rather than in a micellar (below CAC2) or vesicular (above CAC2) suspension, the latter approach being the most obvious to

operate. This piece of information combined to the SAXS data suggests that monomeric adsorption of G-C18:1 at the HC interface competes with, and probably dominates over, its spontaneous self-assembly process in water, whereas the interaction between surfactant monomers and cellulose surface is known to be preferred over micelle-cellulose interactions.<sup>67</sup> If G-C18:1 micelles cannot be thoroughly excluded, they are either below the SAXS detection limit of about 0.3 mg/mL or even possibly adsorbed at the HC interface. Finally, the SAXS data are corroborated by optical microscopy and AFM, which show few large crystallites coexisting with needle-like structures in the supernatant (Figure 3b) and massive amounts of aggregated needle-like structures, reasonably attributed to CNC, in the sub-phase.

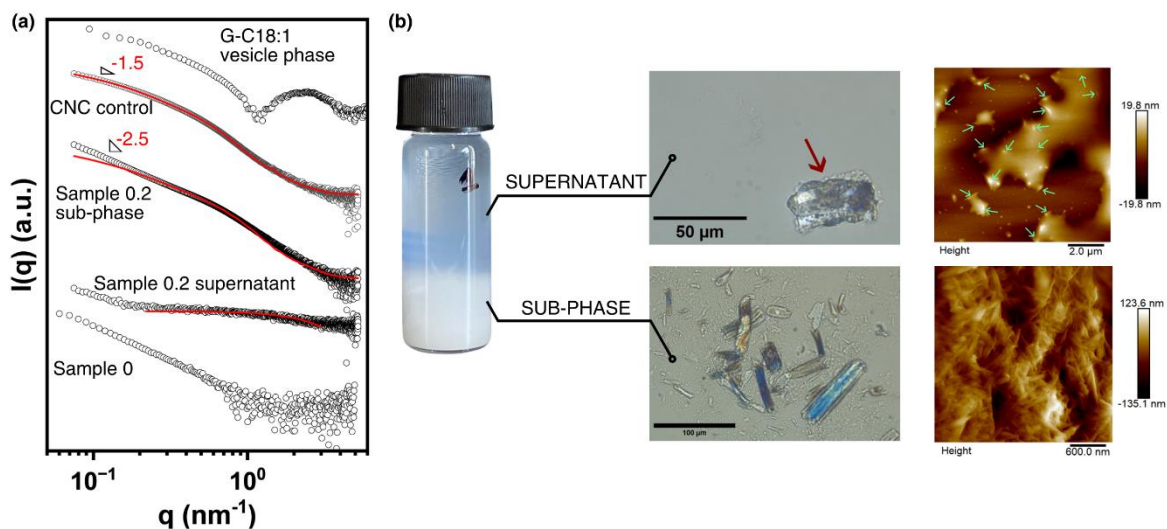


**Figure 3. (a)** SAXS profiles recorded on the supernatant phase and sub-phase of Sample 0.2, HC (G-C18:1 free), sulfated CNC commercial control and G-C18:1 vesicle suspension. All profiles were scaled in the intensity for better reading. The SAXS profiles for all samples are given in the Supporting Information (Figure S6); **(b)** the optical microscope and AFM images of Sample 1.

Zeta potential and SAXS experiments have so far suggested that G-C18:1 adsorbs on the hydrolyzed cellulose and contributing to disperse HC and stabilize CNCs in water. Qualitative and quantitative proof for G-C18:1 adsorption onto cellulose is hereafter established by combining spectroscopic (FTIR) and quartz crystal microbalance with dissipation monitoring (QCM-D) experiments, which can also help understand the mechanism of G-C18:1 adsorption above and below CAC2. It must be noted here that the QCM-D experimental setup requires the use of G-C18:1 solutions, here prepared above CAC1, while the colloidal stabilization experiments

discussed above were optimized with a direct dispersion of G-C18:1 powder to the HC in water. The direct correlation between surface (QCM-D) and bulk (SAXS) data will then be performed with care. To run QCM-D, we prepared a smooth, ultrathin film of cellulose via regeneration of trimethylsilyl cellulose (TMSC), as verified by XPS measurements (Figures S7 and S8). The investigation of biosurfactant adsorption on the cellulose thin film involves monitoring the changes in frequency ( $\Delta f$ ) and dissipation factor ( $\Delta D$ ), here performed at concentrations of 0.2 (below CAC2) and 1 (above CAC2) mg/mL of G-C18:1, as shown in Figure S9.

During the injection of biosurfactant solutions, the change in dissipation remained negligible, with values of  $-0.1 \cdot 10^{-6}$  for Sample 0.2 and  $-0.2 \cdot 10^{-6}$  for Sample 1 (Figure S9b), thus indicating that the adsorbed layer is considered elastic (i.e.,  $\Delta D \leq 1 \cdot 10^{-6}$ ) and its dry mass can be estimated using the Sauerbrey equation.<sup>68</sup> Meanwhile, a significant difference in resonance frequency change ( $\Delta f$ ) was recorded for the two analyzed concentrations of G-C18:1, with the signal settling at -2.55 Hz for Sample 0.2 and -3.01 Hz for Sample 1 after washing out the excess of biosurfactant. These values are considerably lower compared to the frequency changes observed in the adsorption of macromolecules onto cellulose, where frequency shifts can reach signals as high as 30 Hz.<sup>68,69</sup> Using the Sauerbrey equation,<sup>70</sup>  $\Delta f$  can be converted into a mass change,  $\Delta m$ , (Figure 4a) of the adsorbed biosurfactant.

In agreement with the literature,<sup>67</sup> the initial adsorption rate (IAR) of G-C18:1 on cellulose is determined from the slope of  $\Delta m(t)$  at short time scales ( $t < 5$  min) and it is found to be 9 and 35  $\text{ng}/\text{cm}^2 \cdot \text{min}^{-1}$  for concentrations of 0.2 and 1 mg/mL of G-C18:1, respectively. Interestingly, the monotonous increase of the IAR with concentration above the CMC strongly recalls the adsorption of hydrophilic non-ionic ethylene oxide (E) surfactants (e.g., C12E7) onto cellulose rather than that of more hydrophobic ones (e.g., C12E5 or C14E7), of which the IAR is rather constant above their CMC.<sup>67</sup> Indeed, the linear increase of the IAR only occurs below the CMC for all surfactants tested.<sup>67</sup> Moreover, the plateau at the maximum adsorption,  $\tau_{max}$ , (about 57  $\text{ng}/\text{cm}^2$ , that is 1.2  $\mu\text{mol}/\text{m}^2$ ) is reached immediately after the initial adsorption above CAC2 (1 mg/mL) but not yet after 3 hours below CAC2 (0.2 mg/mL), settling at about 30  $\text{ng}/\text{cm}^2$  (0.7  $\mu\text{mol}/\text{m}^2$ ) but still slightly increasing. After rinsing, the irreversible adsorption,  $\tau_i$ , was quantified as 15  $\text{ng}/\text{cm}^2$  (0.3  $\mu\text{mol}/\text{m}^2$ ) at 0.2 mg/mL and 18  $\text{ng}/\text{cm}^2$  (0.4  $\mu\text{mol}/\text{m}^2$ ) at 1 mg/mL (Figure 4b), suggesting that the actual irreversible adsorption of G-C18:1 on the cellulose surface involves the same surfactant's amount, irrespective of its initial aggregation state. The initial to post-rinsing surface concentration ratios,

$\tau_i/\tau_{max}$ , were 50%, with a desorption rate of  $-1.5 \text{ ng/cm}^2\cdot\text{min}^{-1}$ , for the 0.2 mg/mL sample to be compared to 32%, and desorption rate of  $-14 \text{ ng/cm}^2\cdot\text{min}^{-1}$ , for the 1 mg/mL sample. This indicates that higher concentrations of G-C18:1 do not improve its irreversibly adsorbed amount and that increasing the initial G-C18:1 concentration simply causes multilayer adsorption.

Conversion of the typical  $\text{ng/cm}^2$  into  $\mu\text{mol/m}^2$  units allows a direct comparison with adsorption isotherms measured for nonionic ethylene oxide surfactants onto cellulose, which had shown an adsorption of about  $3 \mu\text{mol/m}^2$  of the surfactant at about  $0.5\text{CMC}$ .<sup>71</sup> For the corresponding Sample 0.2, we estimate the adsorption of G-C18:1 at  $0.7 \mu\text{mol/m}^2$ , that is about four times less. At twice the CMC (Sample 1), one finds  $1.2 \mu\text{mol/m}^2$  of G-C18:1, to be compared to about  $5\text{-}6 \mu\text{mol/m}^2$  of ethylene oxide (EO) surfactants, which is about five times less.<sup>71</sup> If these data show that the amount of adsorbed G-C18:1 is objectively less than what was found for EO surfactants, it must be stated that adsorption values of EO surfactants were actually found to be quite high by the authors themselves. Typical plateau values of surfactant adsorption on silica and hydrophobic surfaces were reported to be between 1.5 and 2 times less<sup>72,73</sup> and plateau adsorption of sodium dodecylbenzenesulfonate (NADBS) and Triton X-100 (TX100) onto Whatman-40 ashless filter paper (BET surface area of  $16.5 \text{ m}^2/\text{g}$ ) was rather in the order of  $0.1 \mu\text{mol/m}^2$  for both surfactants (after conversion from published values of  $0.5 \text{ mg/g}$  for NADBS and  $1 \text{ mg/g}$  for TX100).<sup>74</sup> Despite the isotherm study of G-C18:1 onto cellulose was not a goal of this work, the absolute values of adsorption at (pseudo-)equilibrium for Sample 0.2 and Sample 1 are after all in the same order of magnitude as those found for other surfactant systems.<sup>72</sup>

FTIR analysis further demonstrated the irreversible adsorption of G-C18:1 on the cellulose surface. Given that the quantity of biosurfactant used was significantly greater than the amount required for successful irreversible adsorption onto the HC surface, as determined by QCM-D analysis, a dialysis step was implemented to remove any excess biosurfactant from the solution immediately following the mixing of HC and G-C18:1. Figure 4c displays FTIR measurements conducted on dried Sample 1, both with and without dialysis step. HC and G-C18:1 control samples are included for comparison. Given the similarity in chemical composition between cellulose and G-C18:1 (both contain a glycosidic unit), the key distinguishing factor lies in the presence of the C-H stretching vibrations in the 18-carbon chain ( $2854 - 2926 \text{ cm}^{-1}$ ), unsaturated site  $=\text{C-H}$  stretch ( $3010 \text{ cm}^{-1}$ ), and the  $-\text{COOH}$  functional group ( $1701 \text{ cm}^{-1}$ ) in the biosurfactant.<sup>75-77</sup> The peak of  $\text{C}=\text{C}$  stretching vibrations generally appears in the range of  $1620\text{-}1680 \text{ cm}^{-1}$  with medium to weak

intensity, overlapping with the region of strong and sharp C=O stretching peak, making it undetectable.<sup>77</sup> After dialysis, the carbonyl signal at 1701 cm<sup>-1</sup> in the FTIR spectrum indicated persistent G-C18:1 presence. FTIR could also be used to quantitatively characterize the presence of G-C18:1 content.<sup>78</sup> After normalization (see SI), the post-dialysis concentration was found to be 0.38 mg of G-C18:1 adsorbed on the sample after dialysis, in agreement with the previously found amount of biosurfactant needed when analyzing the QCM-D data.<sup>79,80,81</sup>

By subtracting the spectrum of HC from that of Sample 1 after dialysis, one can identify the typical spectral signatures of G-C18:1 (Figure 4d and attribution given in Table S2). FTIR spectroscopy revealed characteristic functional groups indicative of a glycolipid biosurfactant, consistent with previous studies on similar compounds (e.g., from *Azotobacter chroococcum*,<sup>82</sup> *Pseudomonas aeruginosa* DSVP20 and SP4,<sup>83,84</sup> *Bacillus megaterium* SPSW1001<sup>85</sup>). A broad peak at 3389 cm<sup>-1</sup> corresponds to O–H stretching vibrations, consistent with the glucose headgroup of G-C18:1. Peaks at 3010 cm<sup>-1</sup> and 2926 cm<sup>-1</sup> represent aliphatic C–H stretching (CH<sub>2</sub>–CH<sub>3</sub>). The presence of a carbonyl group (C=O) within a carboxylic acid (-COOH) moiety is supported by a peak at 1701 cm<sup>-1</sup> and further confirmed by peaks in the 1420–1323 cm<sup>-1</sup> region, attributable to –OH bending. Finally, the absorption peak at 1030 cm<sup>-1</sup> is attributed to O-C-C stretching, typically observed in the sugar ring.

Spectral subtraction reveals a shift in the O-H stretching vibration from 3389 cm<sup>-1</sup> in the G-C18:1 control to 3340 cm<sup>-1</sup>, indicating the formation of intermolecular hydrogen bonds involving the -OH group of the sugar ring.<sup>79,80</sup> This interaction is further supported by a decrease in intensity of the O-H bending peak at 1075 cm<sup>-1</sup>. Slight frequency shifts are observed for the shoulder (1030–1020 cm<sup>-1</sup>) of the band centered at 1050 cm<sup>-1</sup>. These shifts of the O-C-C stretching and C-O-H bending modes may originate from a modification of the level of hydration of C-O-H groups. Notably, the C=O stretching vibration peak at 1701 cm<sup>-1</sup> remains unchanged, despite the general sensitivity of the C=O band position to carboxylic group interactions.<sup>81</sup> This finding suggests that the primary interaction between G-C18:1 and HC occurs through sugar-sugar interactions, while the biosurfactant tails remain relatively uninfluenced.

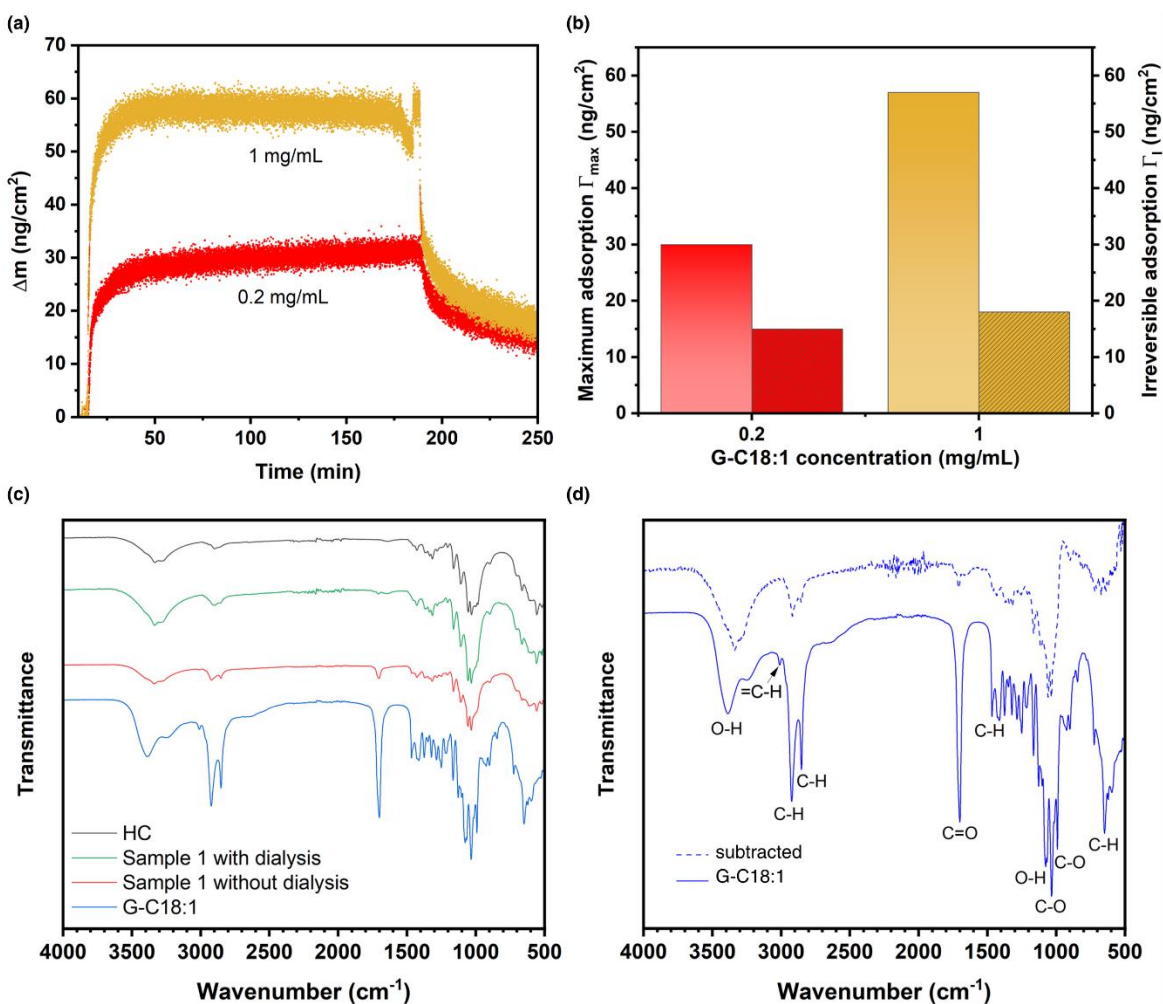


**Figure 4.** (a) QCM-D experiment performed on G-C18:1 (Sample 1 and Sample 2) solution injected onto a home-made cellulose chip. Mass changes were calculated using the Sauerbrey equation  $\Delta m = (-C \cdot \Delta f) / n$ , where  $C$  represents the calibration constant 17.7 ng/cm<sup>2</sup>, and  $n$  (overtone) is equal to 3; (b) maximum and irreversible adsorption yields of G-C18:1 onto cellulose obtained from QCM-D; (c) FTIR measurements were conducted on Sample 1 both before and after dialysis. HC and G-C18:1 control spectra were also provided. (d) Comparison between the FTIR G-C18:1 control spectrum and the Sample 1 spectrum after dialysis (c) to which the HC contribution was subtracted.

### 3. Discussion

Throughout this study, the possible dispersant potential of a single-glucose biosurfactant, G-C18:1, for hydrolyzed cellulose particles has been explored. A significant enhancement in the stability time (up to 2 days) was observed compared to native uncharged cellulose, which otherwise sediments within one hour. For improved colloidal stability, an amount of G-C18:1 in the order of, or lower, than 0.4 mg/mL was detected to be as the suitable amount, that is in the regime of the

G-C18:1's second CAC. Both SAXS and AFM show that the initial HC is converted into a dispersion of aggregated CNCs where the colloidal stability is nevertheless not comparable to sulfate-stabilized CNC, yet. We attribute this fact to several factors. The values of the zeta potential are more negative (slightly less than -20 mV) in the presence of G-C18:1, but not as negative as for sulfate-stabilized CNCs (rather -60 mV).<sup>58</sup> The negative zeta potential values are attributed to the carboxylate group of G-C18:1 ( $pK_a = 5.7$ ),<sup>46</sup> expected to be partially deprotonated at the current  $pH \sim 5$ . According to FTIR argument, the COOH group seems to be less involved in the surface interaction with cellulose if compared to the glucose moiety of G-C18:1. On the other hand, if the calculated G-C18:1-to-CNC mass ratio corresponding to a monolayer of G-C18:1 (using a surface area of  $500 \text{ m}^2/\text{g}$ ) is expected to be in the order of 0.7, the colloidal stability study shows that a mass ratio of 0.4 is not enough while 1 is too much. On this basis, it can be argued that not all the available surface of the initially hydrolyzed cellulose is most likely accessible to G-C18:1.

The actual mechanism of adsorption could also be a matter of debate. It is well-known that surfactant adsorption onto cellulose occurs through the monomeric state of the surfactant, where both the headgroup-cellulose and tail-cellulose interactions are important, although the latter is supposed to play a key role upon the adsorption of G-C18:1. If the tail-cellulose interaction is favored below the CMC, it can also occur above the CMC for hydrophilic surfactants with a high micelle-monomer dissociation rate.<sup>67</sup> In other words, surfactants with high CMC values can efficiently adsorb in the monomer state also above their CMC, while surfactants with low CMC values essentially adsorb predominantly below their CMC. This mechanism was supposed to hold if the affinity between the headgroups and cellulose is low, which was supposed to be true in the case of EO surfactants.<sup>67</sup> In the present case, the CMC of G-C18:1 was reported to be between 0.07 mg/mL and 0.12 mg/mL at physiological pH and 0.035 mg/mL at pH 3,<sup>44-46</sup> the latter verified in this work (CAC1) at pH between 4.5 and 5 by DLS. For G-C18:1, a CAC1 of 0.03 mg/mL is equivalent to  $6.5 \times 10^{-2} \text{ mol/m}^3$ , which is in the order of the CMC of C12E5,<sup>67</sup> suggesting a behavior at the borderline between a slightly hydrophobic (C12E5) and a more hydrophilic (e.g., C12E7, with CMC or  $8.0 \times 10^{-2} \text{ mol/m}^3$ ) surfactant.

Several scenarios could then be proposed in the present work, where G-C18:1 is always above its CAC1. 1) The interactions between the headgroup (glucose) of G-C18:1 and cellulose are negligible and G-C18:1 behaves like a hydrophobic surfactant, like C12E5, characterized by a slow micelle dissociation rate. 2) The interactions between the headgroup of G-C18:1 and cellulose

are negligible and G-C18:1 behaves like a hydrophilic surfactant, similar to C12E7, characterized by a fast micelle dissociation rate. 3) The interactions between the headgroup of G-C18:1 and cellulose are not negligible and G-C18:1 adsorption occurs in its micellar state, possibly through the intermediate of the monomer.

Scenario 1) can easily be excluded because the IAR measured by QCM-D increases with increasing the concentration above CAC1 (Figure 4b). G-C18:1 then rather behaves like C12E7, suggesting scenario 2) more plausible. However, scenario 2), in which the adsorption is driven by the monomeric form of G-C18:1 following a Langmuir monolayer adsorption model,<sup>67,86</sup> and where existing micelles act as a reservoir of matter, could also be questioned. First of all, the CAC1 of G-C18:1 is lower than the CMC of C12E7 and rather comparable with that of C12E5, suggesting that the dissociation rate is most likely slow. Secondly, there is no evidence of a SAXS signal of free micelles (or vesicles), even well above twice the CAC2 (Sample 1), while such a signal should actually be expected according to quantitative arguments. Considering a value of surface area per G-C18:1 in the order of  $50 \text{ \AA}^2/\text{molecule}$ ,<sup>51-53</sup> one can easily estimate the total surface area to be contained between  $2.6$  and  $6.5 \text{ \AA}^2/10^{22}$  for  $0.4 \text{ g}$  and  $1.0 \text{ g}$  of G-C18:1 (per mL of solution). If HC at  $1 \text{ g/mL}$  would be quantitatively transformed into CNCs, one expects between  $4.0$  and  $5.0 \text{ \AA}^2/10^{22}$  available, on the basis of  $400\text{-}500 \text{ m}^2/\text{g}$ .<sup>49,50</sup> Considering that a complete stabilization is never reached in the present case, even in excess of G-C18:1, it goes without saying that the entire theoretical surface area of HC is not accessible. Considering that the best stability is achieved between  $0.2$  and  $0.4 \text{ g}$  (per mL) of G-C18:1, the excess of G-C18:1 in solution is then above  $0.6 \text{ g/mL}$ . On the basis of SAXS arguments recorded on the G-C18:1 control solutions (Figure S6c), one then expects a background scattering attributed to G-C18:1 self-assembly either in the top or bottom phase. This is never the case.

Finally, scenario 3) supposes a non-negligible affinity between the glucose headgroup of G-C18:1, in its monomeric or micellar form, and cellulose, whereas carbohydrate-carbohydrate interactions are well-known in the literature,<sup>87</sup> in particular to explain cell-cell recognition,<sup>88</sup> and also reported for biosurfactants.<sup>89</sup> In the present system, this scenario could be supported by the glucose-cellulose interactions suggested by FTIR data. In this case, the Langmuir monolayer hypothesis behind the adsorption of monomeric surfactants onto a surface may not hold anymore.<sup>67,86</sup> Considering again the fact that G-C18:1 is always introduced above its CAC1, one could suppose the direct interaction between micelles and the cellulose surface. Indeed, as discussed above,

neither micelles nor vesicles are observed in top or bottom phases, even in the excess of G-C18:1, at twice the CAC2. Quantitatively speaking, surface stabilization by micelles, although not directly proven, is not unreasonable. To simplify the problem, we suppose that G-C18:1 micelles are spheres of a total radius of about  $15 \text{ \AA}^{42}$  and aggregation number contained between 20 and 30, in analogy with sophorolipids.<sup>90</sup> Supposing a hexagonal arrangement of the micelles on the surface (packing density of 0.9), one can estimate the occupied surface area by the micelles to be between  $5.5\text{-}8.3 \text{ \AA}^2/10^{22}$  at 1 mg/mL and  $2.2\text{-}3.2 \text{ \AA}^2/10^{22}$  at 0.4 mg/mL. As discussed above, if the entire HC would be transformed into CNC, the total available area would be in the order of  $4\text{-}5 \text{ \AA}^2/10^{22}$ . Despite the crude hypotheses, these values, which should of course be taken as orders of magnitude, show that the total amount of expected G-C18:1 micelles is enough, and actually in excess, to cover the theoretically available surface of CNC. Interestingly, back-calculation of the excess G-C18:1 in solution shows that, if the entire CNC surface would be available, the residual content of G-C18:1 is either not expected or expected below the detection limit of SAXS. For lower accessible CNC surface area, one still does not expect excess G-C18:1 in solution at its CAC2, while one could expect enough to be detected by SAXS for the 1 mg/mL G-C18:1 sample below a threshold CNC surface area.

The considerations above suggest that micelles-HC interactions driven by carbohydrate-carbohydrate interactions are able to disperse HC into aggregated CNCs. However, the actual mechanism could be more complex, deserving more work. Indeed, the stabilization of HC was optimal when G-C18:1 was introduced in a powdery form rather than as a micellar solution. Although hard to compare, QCM-D data, in which G-C18:1 was introduced as a solution above (vesicle phase) and below (micelle phase) CAC2, show that the surface coverage of the cellulose film (assuming a homogeneous coating of the substrate) is only 10%. This is calculated from the value of  $15 \text{ ng/cm}^2$  (value after rinsing) and using the same structural hypotheses discussed above (spherical micelle of  $15 \text{ \AA}$  radius disposed in a hexagonal packing and of aggregation number of 30). A monomer-mediated micellar adsorption process could then be plausible.<sup>91</sup>

While CNCs hold considerable promise for replacing manufactured plastics, producing CNCs on a large scale via concentrated acid hydrolysis poses significant challenges. In this context, we are exploring the potential of using a biosurfactant not only for the liquid acid hydrolysis of CNCs but also for cellulose treated with gaseous HCl, which could offer a greener pathway for large-scale CNCs production. Figure S10 shows the HCl gas cellulose and preliminary stability results using

G-C18:1 as dispersant. Despite the stability results being less impressive than with liquid hydrolyzed cellulose, in the order of 8-10 h, the optimal concentrations of G-C18:1 for improved colloidal stability are always close to CAC2. Further work on the use of gaseous HCl-treated cellulose is undergoing.

#### **4. Conclusion**

This work highlights the use of a glycolipid biosurfactant as surface stabilizer for as-prepared uncharged hydrolyzed cellulose microfibrils, which are free of the classical carboxylate or sulfate surface functional groups. The stabilizing effect of the glycolipid G-C18:1 is observed by mixing the sample powder directly to the water dispersion of HCl hydrolyzed cellulose microcrystals. The most promising effects, consisting in a colloidal stability above 24 h compared to 2 h without the glycolipid, are obtained in the vicinity of the second critical aggregation concentration (CAC2, 0.4 mg/mL) of G-C18:1 for 1 mg/mL of cellulose.

Synchrotron SAXS experiments indicate that in the length scale below 50 nm, G-C18:1 stabilizes individual CNCs, characterized by the typical parallelepiped morphology. Above this size domain, G-C18:1 stabilized CNCs tend to aggregate. FTIR experiments show that the interaction between G-C18:1 and the cellulose surface occurs through sugar-sugar, rather than sugar-COOH, interactions, in agreement with zeta potential experiments, which show a more negative surface charge of the G-C18:1 stabilized CNC as compared to hydrolyzed cellulose microcrystals. The interaction between G-C18:1 and cellulose is eventually demonstrated by QCM-D experiments performed below and above CAC2.

Overall, this work suggests that, compared to standard head-tail surfactants, biosurfactants are of interest alternatives. This could be explained by the concomitant presence of a glycosylated headgroup, which promotes sugar-sugar interactions with the cellulose surface, and an accessible carboxylic acid group, which provides a negative charge, in bolaform shape.

#### **Corresponding Author**

\*E-mail: [eero.kontturi@aalto.fi](mailto:eero.kontturi@aalto.fi)

\*E-mail: [niki.baccile@sorbonne-universite.fr](mailto:niki.baccile@sorbonne-universite.fr)

## Funding Sources

Magnus Ehrnrooth Foundation (Finland) is warmly acknowledged for funding the PhD project. ESRF, the European Synchrotron (Grenoble, France), is kindly acknowledged for its financial support associated to the proposal number MX2572. The French Agence Nationale de la Recherche, project number ANR-22-CE43-0017, is acknowledged for its financial support.

## Acknowledgement

We gratefully acknowledge Aalto University, specifically the OtaNano—Nanomicroscopy Center (Aalto-NMC), for providing facilities and technical support. The European Synchrotron Radiation Facility (ESRF) is acknowledged for supporting the SAXS experiments conducted on the BM29 beamline. We also thank Nicolas SANSON at ESPCI (France) for granting access to the Turbiscan instrument.

## Abbreviations

AFM, atomic force microscopy; CAC, critical aggregation concentration; CMC, critical micelle concentration; CNC, cellulose nanocrystal; DLS, dynamic light scattering; FTIR, Fourier transform infrared; HC, hydrolyzed cellulose; IAR, initial adsorption rate; MCC, microcrystalline cellulose; NADBS, sodium dodecylbenzenesulfonate; QCM-D, quartz crystal microbalance with dissipation monitoring; SAXS, small-angle X-ray scattering; TMSC, trimethylsilyl cellulose.

## References

1. Thomas B, Raj MC, Athira BK, et al. Nanocellulose, a Versatile Green Platform: From Biosources to Materials and Their Applications. *Chem Rev.* 2018;118(24):11575-11625. doi:10.1021/acs.chemrev.7b00627
2. Klemm D, Kramer F, Moritz S, et al. Nanocelluloses: A New Family of Nature-Based Materials. *Angewandte Chemie International Edition.* 2011;50(24):5438-5466. doi:10.1002/anie.201001273
3. Dufresne A. *Nanocellulose: From Nature to High Performance Tailored Materials.*; 2012. doi:10.1515/hf-2013-0027
4. Rånby BG, Banderet A, Sillén LG. Aqueous Colloidal Solutions of Cellulose Micelles. *Acta Chem Scand.* 1949;3:649-650. doi:10.3891/acta.chem.scand.03-0649

5. Clarkson CM, El Awad Azrak SM, Forti ES, Schueneman GT, Moon RJ, Youngblood JP. Recent Developments in Cellulose Nanomaterial Composites. *Advanced Materials*. 2021;33(28). doi:10.1002/adma.202000718
6. Parker RM, Guidetti G, Williams CA, et al. The Self-Assembly of Cellulose Nanocrystals: Hierarchical Design of Visual Appearance. *Advanced Materials*. 2018;30(19). doi:10.1002/adma.201704477
7. Heise K, Kontturi E, Allahverdiyeva Y, et al. Nanocellulose: Recent Fundamental Advances and Emerging Biological and Biomimicking Applications. *Advanced Materials*. 2021;33(3). doi:10.1002/adma.202004349
8. Kontturi E, Laaksonen P, Linder MB, et al. Advanced Materials through Assembly of Nanocelluloses. *Advanced Materials*. 2018;30(24). doi:10.1002/adma.201703779
9. Nagarajan KJ, Ramanujam NR, Sanjay MR, et al. *A Comprehensive Review on Cellulose Nanocrystals and Cellulose Nanofibers: Pretreatment, Preparation, and Characterization*. Vol 42.; 2021. doi:10.1002/pc.25929
10. Rana AK, Frollini E, Thakur VK. Cellulose nanocrystals: Pretreatments, preparation strategies, and surface functionalization. *Int J Biol Macromol*. 2021;182:1554-1581. doi:10.1016/j.ijbiomac.2021.05.119
11. Rånby BG. Fibrous macromolecular systems. Cellulose and muscle. The colloidal properties of cellulose micelles. *Discuss Faraday Soc*. 1951;11(0):158-164. doi:10.1039/DF9511100158
12. Hao Z, Hamad WY, Yaseneva P. Understanding the environmental impacts of large-scale cellulose nanocrystals production: Case studies in regions dependent on renewable and fossil fuel energy sources. *Chemical Engineering Journal*. 2023;478:147160. doi:10.1016/j.cej.2023.147160
13. Wang Y, Liu H, Wang Q, et al. Recent advances in sustainable preparation of cellulose nanocrystals via solid acid hydrolysis: A mini-review. *Int J Biol Macromol*. 2023;253:127353. doi:10.1016/j.ijbiomac.2023.127353
14. Hamad WY, Hu TQ. Structure–process–yield interrelations in nanocrystalline cellulose extraction. *Can J Chem Eng*. 2010;88(3):392-402. doi:10.1002/cjce.20298
15. Vanderfleet OM, Reid MS, Bras J, et al. Insight into thermal stability of cellulose nanocrystals from new hydrolysis methods with acid blends. *Cellulose*. 2019;26(1):507-528. doi:10.1007/s10570-018-2175-7
16. Roman M, Winter WT. Effect of Sulfate Groups from Sulfuric Acid Hydrolysis on the Thermal Degradation Behavior of Bacterial Cellulose. Published online 2004. doi:10.1021/bm034519
17. Hindi S, Hindi SSZ. Microcrystalline cellulose: Its processing and pharmaceutical specifications. *BioCrystals Journal*. 2016;1(1):26-38. <https://www.researchgate.net/publication/299594912>

18. Dong XM, Revol JF, Gray DG. Effect of microcrystallite preparation conditions on the formation of colloid crystals of cellulose. *Cellulose*. 1998;5(1):19-32. doi:10.1023/A:1009260511939
19. Araki J, Wada M, Kuga S, Okano T. Flow properties of microcrystalline cellulose suspension prepared by acid treatment of native cellulose. *Colloids Surf A Physicochem Eng Asp*. 1998;142(1):75-82. doi:10.1016/S0927-7757(98)00404-X
20. Wang Y, Wang X, Xie Y, Zhang K. Functional nanomaterials through esterification of cellulose: a review of chemistry and application. *Cellulose*. 2018;25(7):3703-3731. doi:10.1007/s10570-018-1830-3
21. Li D, Henschen J, Ek M. Esterification and hydrolysis of cellulose using oxalic acid dihydrate in a solvent-free reaction suitable for preparation of surface-functionalised cellulose nanocrystals with high yield. *Green Chemistry*. 2017;19(23):5564-5567. doi:10.1039/c7gc02489d
22. Berlioz S, Molina-Boisseau S, Nishiyama Y, Heux L. Gas-Phase Surface Esterification of Cellulose Microfibrils and Whiskers. *Biomacromolecules*. 2009;10(8):2144-2151. doi:10.1021/bm900319k
23. Fraschini C, Chauve G, Bouchard J. TEMPO-mediated surface oxidation of cellulose nanocrystals (CNCs). *Cellulose*. 2017;24(7):2775-2790. doi:10.1007/s10570-017-1319-5
24. Cao X, Ding B, Yu J, Al-Deyab SS. Cellulose nanowhiskers extracted from TEMPO-oxidized jute fibers. *Carbohydr Polym*. 2012;90(2):1075-1080. doi:10.1016/j.carbpol.2012.06.046
25. Cohen N, Ochbaum G, Levi-Kalisman Y, Bitton R, Yerushalmi-Rozen R. Polymer-Induced Modification of Cellulose Nanocrystal Assemblies in Aqueous Suspensions. *ACS Appl Polym Mater*. 2020;2(2):732-740. doi:10.1021/acsapm.9b01048
26. Laitinen O, Hartmann R, Sirviö JA, et al. Alkyl aminated nanocelluloses in selective flotation of aluminium oxide and quartz. *Chem Eng Sci*. 2016;144:260-266. doi:10.1016/J.CES.2016.01.052
27. Fang W, Arola S, Malho JM, Kontturi E, B. Linder M, Laaksonen P. Noncovalent Dispersion and Functionalization of Cellulose Nanocrystals with Proteins and Polysaccharides. *Biomacromolecules*. 2016;17(4):1458-1465. doi:10.1021/acs.biomac.6b00067
28. Song Z, Xiao H, Zhao Y. Hydrophobic-modified nano-cellulose fiber/PLA biodegradable composites for lowering water vapor transmission rate (WVTR) of paper. *Carbohydr Polym*. 2014;111:442-448. doi:10.1016/J.CARBPOL.2014.04.049
29. Salajková M, Berglund LA, Zhou Q. Hydrophobic cellulose nanocrystals modified with quaternary ammonium salts. *J Mater Chem*. 2012;22(37):19798-19805. doi:10.1039/c2jm34355j

30. Shang Z, An X, Seta FT, et al. Improving dispersion stability of hydrochloric acid hydrolyzed cellulose nano-crystals. *Carbohydr Polym.* 2019;222(March):115037. doi:10.1016/j.carbpol.2019.115037
31. Tardy BL, Yokota S, Ago M, et al. Nanocellulose–surfactant interactions. *Curr Opin Colloid Interface Sci.* 2017;29:57-67. doi:10.1016/j.cocis.2017.02.004
32. Banat IM, Makkar RS, Cameotra SS. *MINI-REVIEW Potential Commercial Applications of Microbial Surfactants.*
33. Singh A, Van Hamme JD, Ward OP. Surfactants in microbiology and biotechnology: Part 2. Application aspects. *Biotechnol Adv.* 2007;25(1):99-121. doi:10.1016/j.biotechadv.2006.10.004
34. Ruby Aslam MMJASZ. *Advancements in Biosurfactants Research.* Vol 978-3-031-21682-4. (Ruby Aslam MMJASZ, ed.). Springer Cham; 2023.
35. Adetunji AI, Olaniran AO. Production and potential biotechnological applications of microbial surfactants: An overview. *Saudi J Biol Sci.* 2021;28(1):669-679. doi:10.1016/j.sjbs.2020.10.058
36. Hoja J, J. Maurer R, F. Sax A. Adsorption of Glucose, Cellobiose, and Cellotetraose onto Cellulose Model Surfaces. *J Phys Chem B.* 2014;118(30):9017-9027. doi:10.1021/jp5025685
37. Peri S, Muthukumar L, Nazmul Karim M, Khare R. Dynamics of cello-oligosaccharides on a cellulose crystal surface. *Cellulose.* 2012;19(6):1791-1806. doi:10.1007/s10570-012-9771-8
38. Niinivaara E, M. Vanderfleet O, Kontturi E, D. Cranston E. Tuning the Physicochemical Properties of Cellulose Nanocrystals through an In Situ Oligosaccharide Surface Modification Method. *Biomacromolecules.* 2021;22(8):3284-3296. doi:10.1021/acs.biomac.1c00384
39. Majoinen J, S. Haataja J, Appelhans D, et al. Supracolloidal Multivalent Interactions and Wrapping of Dendronized Glycopolymers on Native Cellulose Nanocrystals. *J Am Chem Soc.* 2014;136(3):866-869. doi:10.1021/ja411401r
40. D. Klemm BPTHUHW. *Comprehensive Cellulose Chemistry.* Vol Vol. 1. Wiley-VCH, Weinheim; 1998.
41. Baccile N, Poirier A, Seyrig C, et al. Chameleonic amphiphile: The unique multiple self-assembly properties of a natural glycolipid in excess of water. *J Colloid Interface Sci.* 2023;630:404-415. doi:10.1016/j.jcis.2022.07.130
42. Baccile N, Cuvier AS, Prévost S, et al. Self-Assembly Mechanism of pH-Responsive Glycolipids: Micelles, Fibers, Vesicles, and Bilayers. *Langmuir.* 2016;32(42):10881-10894. doi:10.1021/acs.langmuir.6b02337

43. Baccile N, Selmane M, Le Griel P, et al. PH-Driven Self-Assembly of Acidic Microbial Glycolipids. *Langmuir*. 2016;32(25):6343-6359. doi:10.1021/acs.langmuir.6b00488
44. Ishigami Y, GY, SY et al. Interfacial and micellar behavior of glucose lipid. *Biotechnol Lett*. 1994;16:593-598.
45. Imura T, Masuda Y, Minamikawa H, et al. *Enzymatic Conversion of Diacetylated Sophorolipid into Acetylated Glucoselipid: Surface-Active Properties of Novel Bolaform Biosurfactants*. Vol 59.; 2010. <http://www.jstage.jst.go.jp/browse/jos/>
46. Cui T, Tang Y, Zhao M, Hu Y, Jin M, Long X. Preparing Biosurfactant Glucolipids from Crude Sophorolipids via Chemical Modifications and Their Potential Application in the Food Industry. *J Agric Food Chem*. 2023;71(6):2964-2974. doi:10.1021/acs.jafc.2c06066
47. Bergström LM. Explaining the growth behavior of surfactant micelles. *J Colloid Interface Sci*. 2015;440:109-118. doi:10.1016/j.jcis.2014.10.054
48. Leng J, Egelhaaf SU, Cates ME. Kinetics of the Micelle-to-Vesicle Transition: Aqueous Lecithin-Bile Salt Mixtures. *Biophys J*. 2003;85(3):1624-1646. doi:10.1016/S0006-3495(03)74593-7
49. Brinkmann A, Chen M, Couillard M, Jakubek ZJ, Leng T, Johnston LJ. Correlating Cellulose Nanocrystal Particle Size and Surface Area. *Langmuir*. 2016;32(24):6105-6114. doi:10.1021/acs.langmuir.6b01376
50. Heath L, Thielemans W. Cellulose nanowhisker aerogels. *Green Chemistry*. 2010;12(8):1448. doi:10.1039/c0gc00035c
51. Rau U, Heckmann R, Wray V, Lang S. Enzymatic conversion of a sophorolipid into a glucose lipid. *Biotechnol Lett*. 1999;21(11):973-977. doi:10.1023/A:1005665222976
52. Ericsson CA, Söderman O, Garamus VM, Bergström M, Ulvenlund S. Effects of Temperature, Salt, and Deuterium Oxide on the Self-Aggregation of Alkylglycosides in Dilute Solution. 1. n-Nonyl- $\beta$ -D-glucoside. *Langmuir*. 2004;20(4):1401-1408. doi:10.1021/la035613e
53. Shinoda K, Yamaguchi T, Hori R. The Surface Tension and the Critical Micelle Concentration in Aqueous Solution of  $\beta$ -D-Alkyl Glucosides and their Mixtures. *Bull Chem Soc Jpn*. 1961;34(2):237-241. doi:10.1246/bcsj.34.237
54. Heux L, Chauve G, Bonini C. Nonflocculating and chiral-nematic self-ordering of cellulose microcrystals suspensions in nonpolar solvents. *Langmuir*. 2000;16(21):8210-8212. doi:10.1021/la9913957
55. Vanderfleet OM, Cranston ED. Production routes to tailor the performance of cellulose nanocrystals. *Nat Rev Mater*. 2021;6(2):124-144. doi:10.1038/s41578-020-00239-y
56. Chu Y, Sun Y, Wu W, Xiao H. Dispersion Properties of Nanocellulose: A Review. *Carbohydr Polym*. 2020;250(June):116892. doi:10.1016/j.carbpol.2020.116892

57. Bhattacharjee S. DLS and zeta potential – What they are and what they are not? *Journal of Controlled Release*. 2016;235:337-351. doi:10.1016/J.JCONREL.2016.06.017
58. Levanič J, Petrovič Šenk V, Nadrah P, Poljanšek I, Oven P, Haapala A. Analyzing TEMPO-Oxidized Cellulose Fiber Morphology: New Insights into Optimization of the Oxidation Process and Nanocellulose Dispersion Quality. *ACS Sustainable Chemistry & Engineering*. 2020;8(48):17752-17762. doi:10.1021/acssuschemeng.0c05989
59. Jordan JH, Eason MW, Condon BD. Alkali hydrolysis of sulfated cellulose nanocrystals: Optimization of reaction conditions and tailored surface charge. *Nanomaterials*. 2019;9(9). doi:10.3390/nano9091232
60. Grachev V, Deschaume O, Lang PR, Lettinga MP, Bartic C, Thielemans W. Dimensions of Cellulose Nanocrystals from Cotton and Bacterial Cellulose: Comparison of Microscopy and Scattering Techniques. *Nanomaterials*. 2024;14(5). doi:10.3390/nano14050455
61. Leppänen K, Pirkkalainen K, Penttilä P, Sievänen J, Kotelnikova N, Serimaa R. Small-angle x-ray scattering study on the structure of microcrystalline and nanofibrillated cellulose. In: *Journal of Physics: Conference Series*. Vol 247. Institute of Physics Publishing; 2010. doi:10.1088/1742-6596/247/1/012030
62. Wang Z, Li P, Ma K, et al. The structure of alkyl ester sulfonate surfactant micelles: The impact of different valence electrolytes and surfactant structure on micelle growth. *J Colloid Interface Sci*. 2019;557:124-134. doi:10.1016/j.jcis.2019.09.016
63. Von O. G LATTER, O. K RATKY. *Small Angle X-ray Scattering*. (Academic Press, ed.); 1982. doi:10.1002/actp.1985.010360520
64. A. Sacui I, C. Nieuwendaal R, J. Burnett D, et al. Comparison of the Properties of Cellulose Nanocrystals and Cellulose Nanofibrils Isolated from Bacteria, Tunicate, and Wood Processed Using Acid, Enzymatic, Mechanical, and Oxidative Methods. *ACS Applied Materials & Interfaces*. 2014;6(9):6127-6138. doi:10.1021/am500359f
65. Teixeira J. Small-angle scattering by fractal systems. *J Appl Crystallogr*. 1988;21(6):781-785. doi:10.1107/S0021889888000263
66. Cherhal F, Cousin F, Capron I. Influence of Charge Density and Ionic Strength on the Aggregation Process of Cellulose Nanocrystals in Aqueous Suspension, as Revealed by Small-Angle Neutron Scattering. *Langmuir*. 2015;31(20):5596-5602. doi:10.1021/acs.langmuir.5b00851
67. Torn LH, Koopal LK, de Keizer A, Lyklema J. Adsorption of Nonionic Surfactants on Cellulose Surfaces: Adsorbed Amounts and Kinetics. *Langmuir*. 2005;21(17):7768-7775. doi:10.1021/la051102b
68. S. Kontturi K, Solhi L, Kontturi E, Tammelin T. Adsorption of Polystyrene from Theta Condition on Cellulose and Silica Studied by Quartz Crystal Microbalance. *Langmuir*. 2023;0(0). doi:10.1021/acs.langmuir.3c02777

69. Griffo A, Hähl H, Grandthyll S, et al. Single-Molecule Force Spectroscopy Study on Modular Resilin Fusion Protein. *ACS Omega*. 2017;2(10):6906-6915. doi:10.1021/acsomega.7b01133
70. D. Vogt B, K. Lin E, Wu W li, C. White C. Effect of Film Thickness on the Validity of the Sauerbrey Equation for Hydrated Polyelectrolyte Films. *J Phys Chem B*. 2004;108(34):12685-12690. doi:10.1021/jp0481005
71. Torn LH, Koopal LK, de Keizer A, Lyklema J. Adsorption of Nonionic Surfactants on Cellulose Surfaces: Adsorbed Amounts and Kinetics. *Langmuir*. 2005;21(17):7768-7775. doi:10.1021/la051102b
72. Kronberg B, Stenius P. The effect of surface polarity on the adsorption of nonionic surfactants. I. Thermodynamic considerations. *J Colloid Interface Sci*. 1984;102(2):410-417. doi:10.1016/0021-9797(84)90243-1
73. Bohmer MR, Koopal LK, Janssen R, Lee EM, Thomas RK, Rennie AR. Adsorption of nonionic surfactants on hydrophilic surfaces. An experimental and theoretical study on association in the adsorbed layer. *Langmuir*. 1992;8(9):2228-2239. doi:10.1021/la00045a027
74. Paria S, Manohar C, Khilar KC. Adsorption of anionic and non-ionic surfactants on a cellulosic surface. *Colloids Surf A Physicochem Eng Asp*. 2005;252(2-3):221-229. doi:10.1016/j.colsurfa.2004.09.022
75. Zimudzi TJ, Feldman KE, Sturnfield JF, Roy A, Hickner MA, Stafford CM. Quantifying Carboxylic Acid Concentration in Model Polyamide Desalination Membranes via Fourier Transform Infrared Spectroscopy. *Macromolecules*. 2018;51(17):6623-6629. doi:10.1021/acs.macromol.8b01194
76. Max JJ, Chapados C. Infrared Spectroscopy of Aqueous Carboxylic Acids: Comparison between Different Acids and Their Salts. *J Phys Chem A*. 2004;108(16):3324-3337. doi:10.1021/jp036401t
77. Coates J. Interpretation of Infrared Spectra, A Practical Approach. In: *Encyclopedia of Analytical Chemistry*. Wiley; 2000. doi:10.1002/9780470027318.a5606
78. Hong T, Yin JY, Nie SP, Xie MY. Applications of infrared spectroscopy in polysaccharide structural analysis: Progress, challenge and perspective. *Food Chem X*. 2021;12:100168. doi:10.1016/j.fochx.2021.100168
79. Guo L, Sato H, Hashimoto T, Ozaki Y. FTIR Study on Hydrogen-Bonding Interactions in Biodegradable Polymer Blends of Poly(3-hydroxybutyrate) and Poly(4-vinylphenol). *Macromolecules*. 2010;43(8):3897-3902. doi:10.1021/ma100307m
80. Mekonnen KD. Fourier transform infrared spectroscopy as a tool for identifying the unique characteristic bands of lipid in oilseed components: Confirmed via Ethiopian indigenous desert date fruit. *Heliyon*. 2023;9(4):e14699. doi:10.1016/j.heliyon.2023.e14699

81. Hay MB, Myneni SCB. Structural environments of carboxyl groups in natural organic molecules from terrestrial systems. Part 1: Infrared spectroscopy. *Geochim Cosmochim Acta*. 2007;71(14):3518-3532. doi:10.1016/j.gca.2007.03.038
82. Thavasi R, Subramanyam Nambaru VRM, Jayalakshmi S, Balasubramanian T, Banat IM. Biosurfactant Production by *Azotobacter chroococcum* Isolated from the Marine Environment. *Marine Biotechnology*. 2009;11(5):551-556. doi:10.1007/s10126-008-9162-1
83. Pornsunthorntawe O, Wongpanit P, Chavadej S, Abe M, Rujiravanit R. Structural and physicochemical characterization of crude biosurfactant produced by *Pseudomonas aeruginosa* SP4 isolated from petroleum-contaminated soil. *Bioresour Technol*. 2008;99(6):1589-1595. doi:10.1016/j.biortech.2007.04.020
84. Singh N, Pemmaraju SC, Pruthi PA, Cameotra SS, Pruthi V. Candida Biofilm Disrupting Ability of Di-rhamnolipid (RL-2) Produced from *Pseudomonas aeruginosa* DSVP20. *Appl Biochem Biotechnol*. 2013;169(8):2374-2391. doi:10.1007/s12010-013-0149-7
85. Singh V, Waris Z, Banat IM, Saha S, Padmanabhan P. Assessment of Rheological Behaviour of Water-in-Oil Emulsions Mediated by Glycolipid Biosurfactant Produced by *Bacillus megaterium* SPSW1001. *Appl Biochem Biotechnol*. 2022;194(3):1310-1326. doi:10.1007/s12010-021-03717-3
86. Wang J, Guo X. Adsorption kinetic models: Physical meanings, applications, and solving methods. *J Hazard Mater*. 2020;390:122156. doi:10.1016/j.jhazmat.2020.122156
87. Kav B, Grafmüller A, Schneck E, Weigl TR. Weak carbohydrate-carbohydrate interactions in membrane adhesion are fuzzy and generic. *Nanoscale*. 2020;12(33):17342-17353. doi:10.1039/D0NR03696J
88. Bucior I, Scheuring S, Engel A, Burger MM. Carbohydrate-carbohydrate interaction provides adhesion force and specificity for cellular recognition. *J Cell Biol*. 2004;165(4):529-537. doi:10.1083/jcb.200309005
89. Rondelli V, Mollica L, Koutsioubas A, et al. Carbohydrate-carbohydrate interaction drives the preferential insertion of dirhamnolipid into glycosphingolipid enriched membranes. *J Colloid Interface Sci*. 2022;616:739-748. doi:10.1016/j.jcis.2022.02.120
90. Manet S, Cuvier AS, Valotteau C, et al. Structure of Bolaamphiphile Sophorolipid Micelles Characterized with SAXS, SANS, and MD Simulations. *Journal of Physical Chemistry B*. 2015;119(41):13113-13133. doi:10.1021/acs.jpcc.5b05374
91. Kong L, Saar KL, Jacquat R, et al. Mechanism of biosurfactant adsorption to oil/water interfaces from millisecond scale tensiometry measurements. *Interface Focus*. 2017;7(6):20170013. doi:10.1098/rsfs.2017.0013

# Table of Contents

